Paleoceanography and Paleoclimatology

Supporting Information for

High-latitude, Indian Ocean, and orbital influences on eastern African hydroclimate across the Plio-Pleistocene boundary

Bryce A. Mitsunaga[1], Rachel L. Lupien[2], Samantha Ouertani[1], Brandon Stubbs[1], Alan L. Deino[3], John D. Kingston[4], Mona Stockhecke[5], Erik T. Brown[5], and James M. Russell[1]

[1]Department of Earth, Environmental, and Planetary Sciences, Brown University, Providence, USA. [2]Department of Geoscience, Aarhus University, Aarhus, Denmark. [3]Berkeley Geochronology Center, Berkeley, USA. [4]Department of Anthropology, University of Michigan, Ann Arbor, USA. [5]Large Lakes Observatory, University of Minnesota Duluth, Duluth, USA.

Contents of this file

Figures S1 to S9
References

Introduction

Supplementary figures include spectral analyses and tests of HSPDP-BTB13-1A ("BTB13") proxy data as well as sea surface temperature records mentioned in the text.

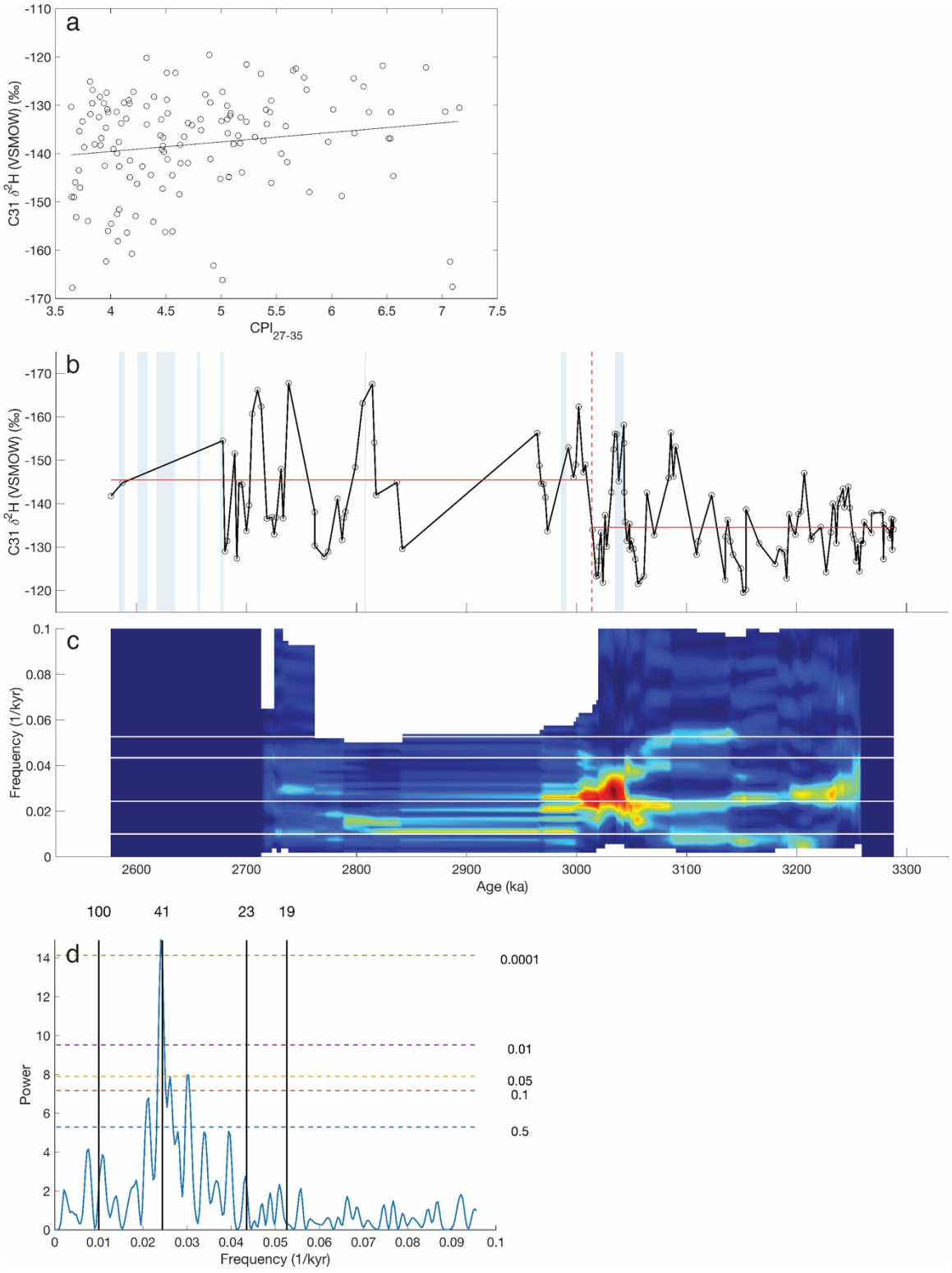

Figure S1. Analyses of BTB13 δ^2H_{C31} values after excluding low-$CPI_{27\text{-}35}$ value (< 3.628) samples. (a) BTB13 $CPI_{27\text{-}35}$ versus δ^2H_{C31} values (n = 137, r = 0.16, p < 0.1). (b) BTB13 δ^2H_{C31} values. Vertical dashed red lines show the location of the single most abrupt shift in mean (red). Solid horizontal red lines show mean values before and after the

changepoint. Blue bars denote significant diatomite strata D_1-D_8 (Westover et al., 2021). (c) 28-point evolutionary Lomb-Scargle periodogram of δ^2H_{C31} values. (d) Lomb-Scargle power spectra of δ^2H_{C31} values. Dashed lines denote false alarm probability.

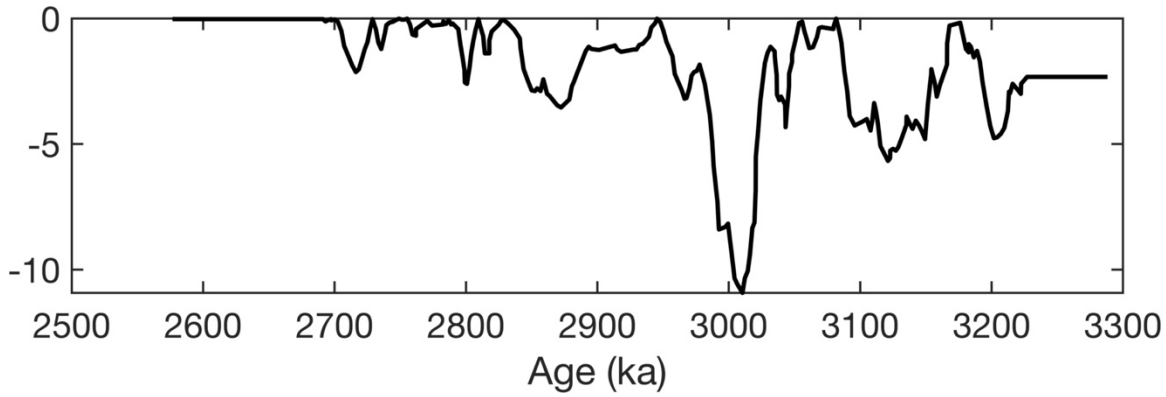

Figure S2. Seventy-point running Mann-Whitney test of BTB13 δ^2H_{C31} values.

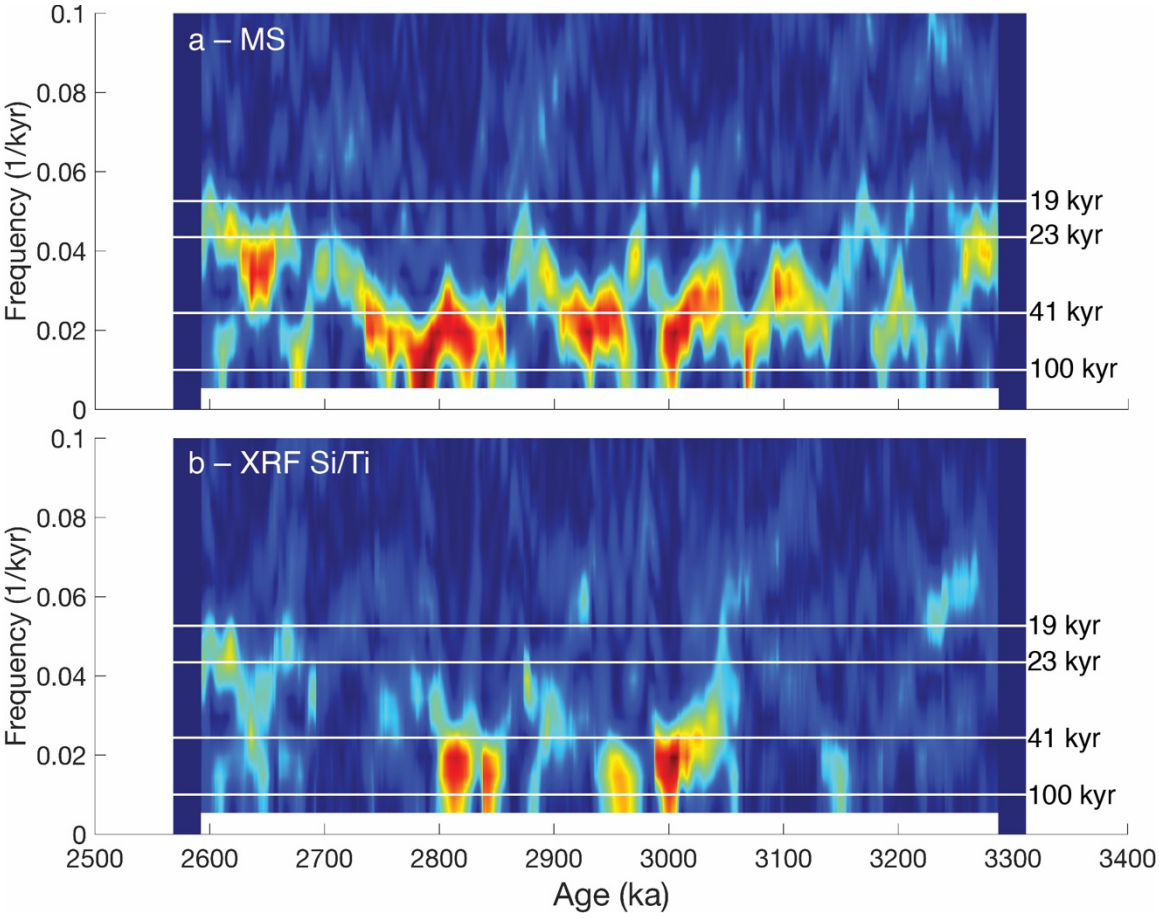

Figure S3. Evolutionary Lomb-Scargle periodogram (50-point window) of BTB13 A) ln magnetic susceptibility and B) XRF Si/Ti.

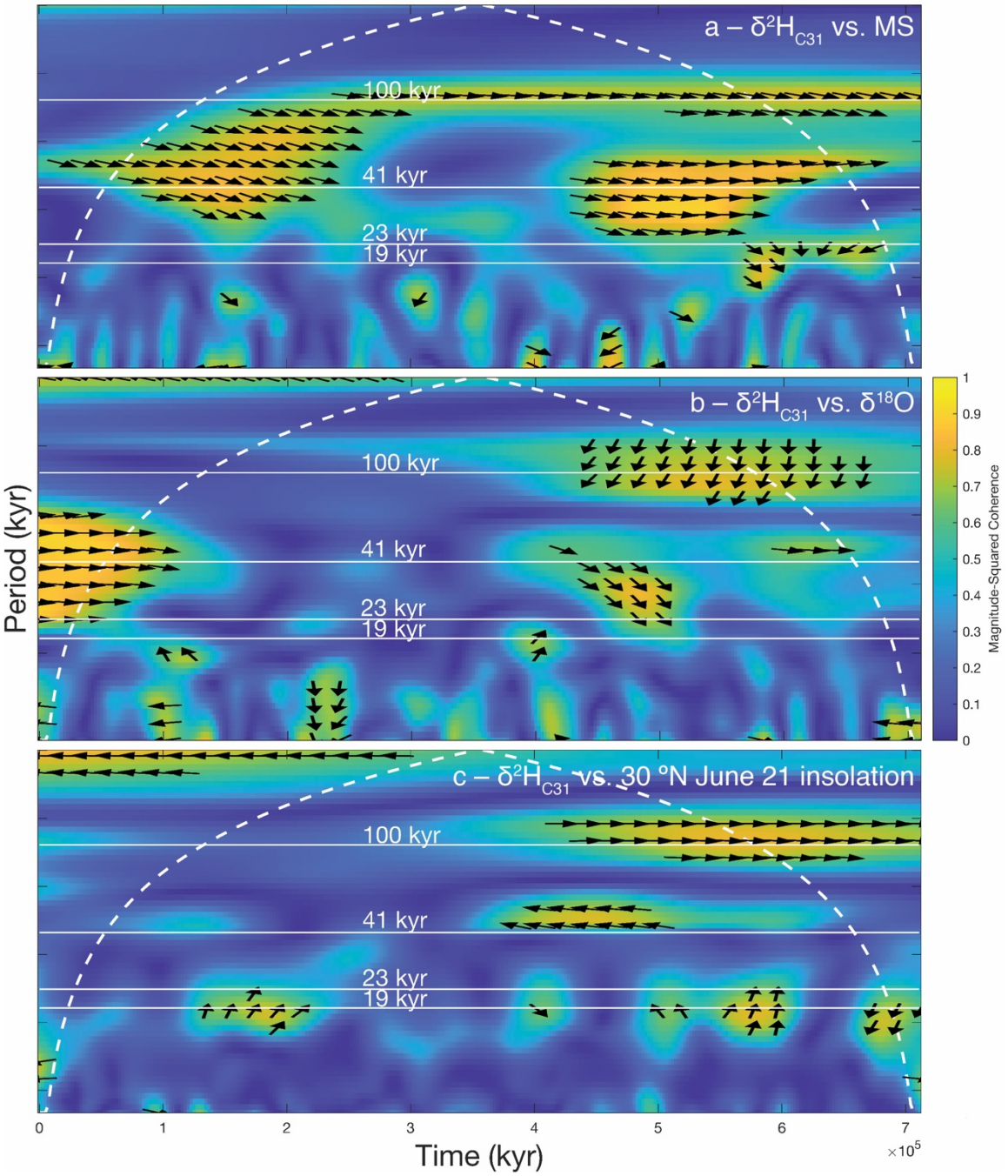

Figure S4. Wavelet cross-spectra of BTB13 δ^2H_{C31} values and (a) ln magnetic susceptibility, (b) global benthic $\delta^{18}O$ values, and (c) June 21st insolation at 30 °N. Dashed white line denotes cone of influence. Arrows (≥ 0.60 magnitude-squared coherence) pointing to the (a) right, (b) right, and (c) left indicate 0° phase lead / lag.

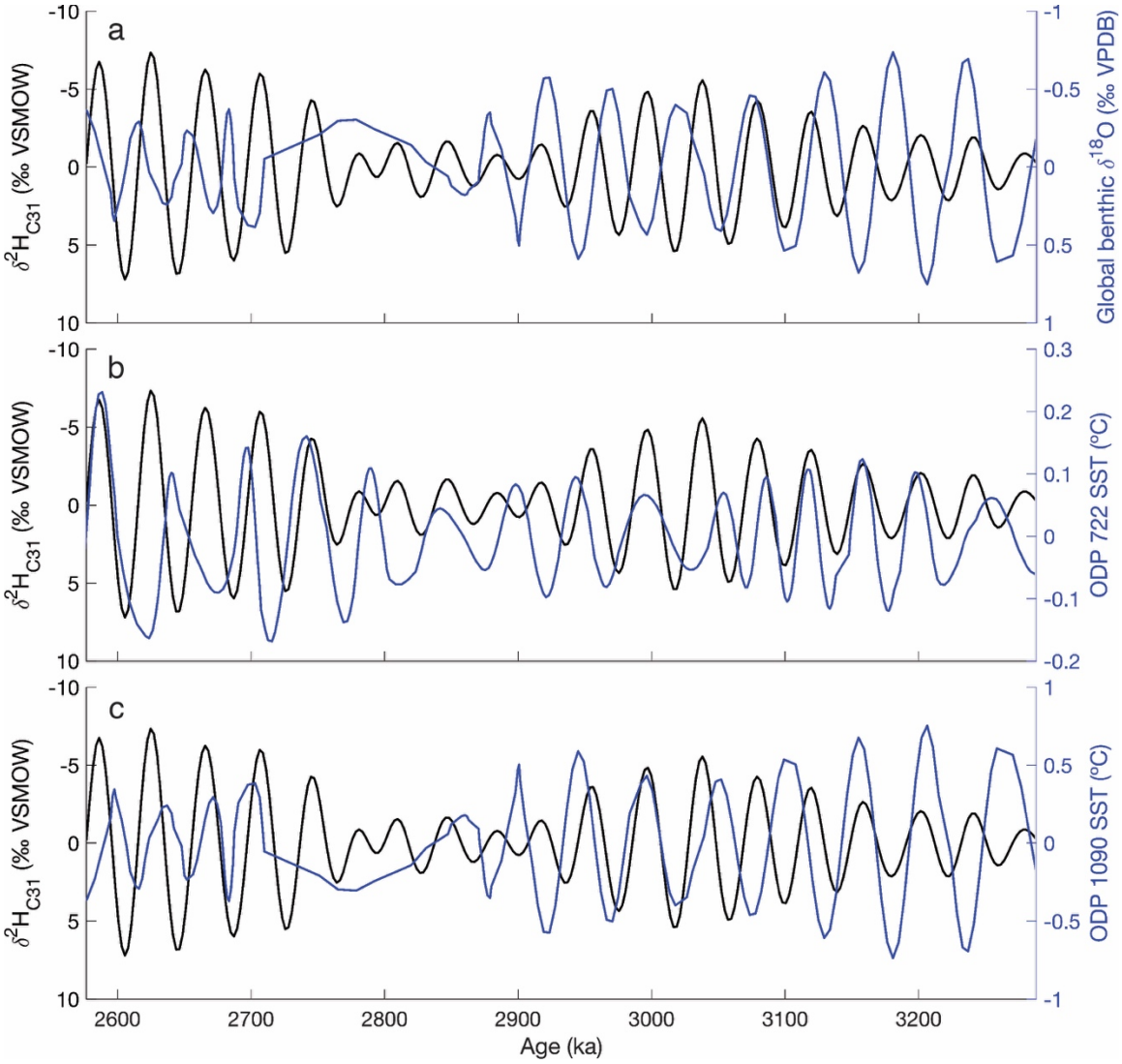

Figure S5. 41 kyr bandpass filtered BTB13 δ^2H_{C31} values (black) and (a) global benthic foraminiferal $\delta^{18}O$ values (Lisiecki & Raymo, 2005) and (b) Arabian Sea (Herbert et al., 2015) and (c) Southern Ocean SSTs (Martínez-Garcia et al., 2010).

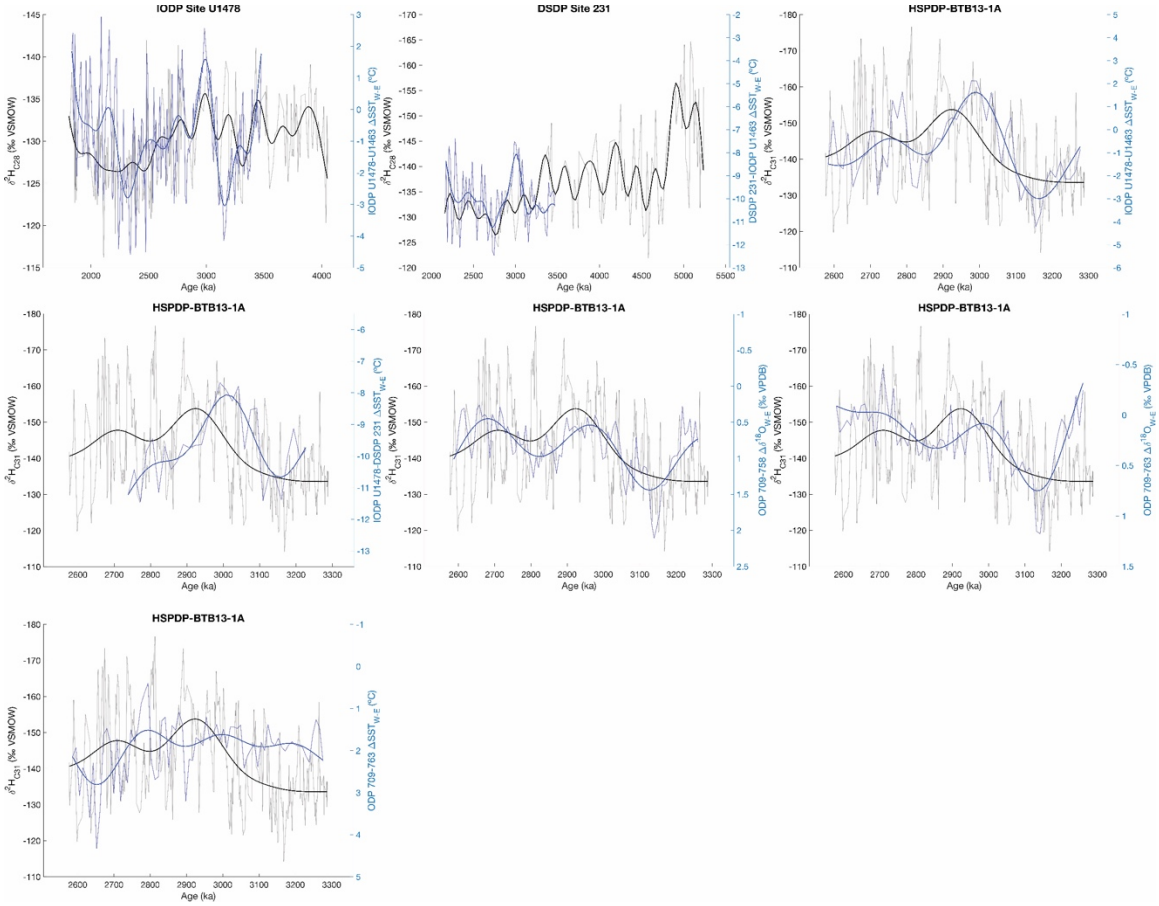

Figure S6. Plio-Pleistocene hydroclimate proxy (black) and Indian Ocean ΔSST_{W-E} (blue) time series. 200-kyr low-pass sixth order Butterworth filter in bold. All y-axes are oriented such that values interpreted as higher moisture availability and temperature are upwards.

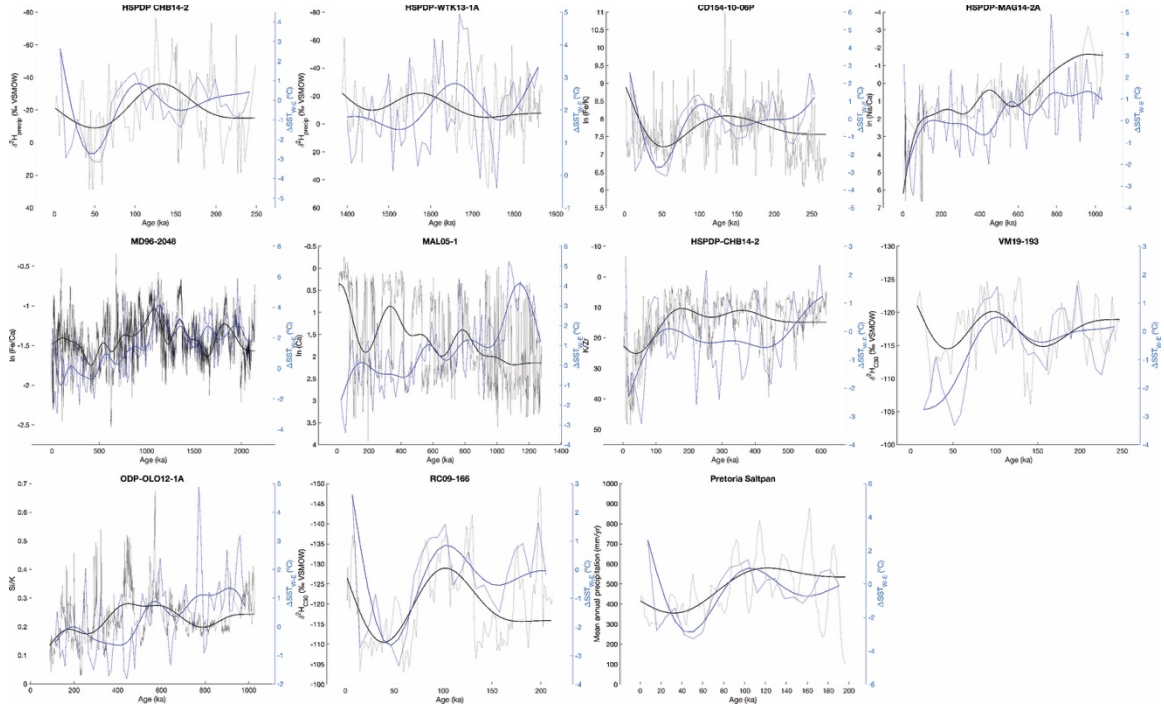

Figure S7. Pleistocene-Holocene hydroclimate proxy (black) and Indian Ocean ΔSST_{W-E} (blue) time series. 100- (<250-kyr records) or 200-kyr (>250-kyr records) low-pass sixth order Butterworth filter in bold. All y-axes are oriented such that values interpreted as higher moisture availability and temperature are upwards.

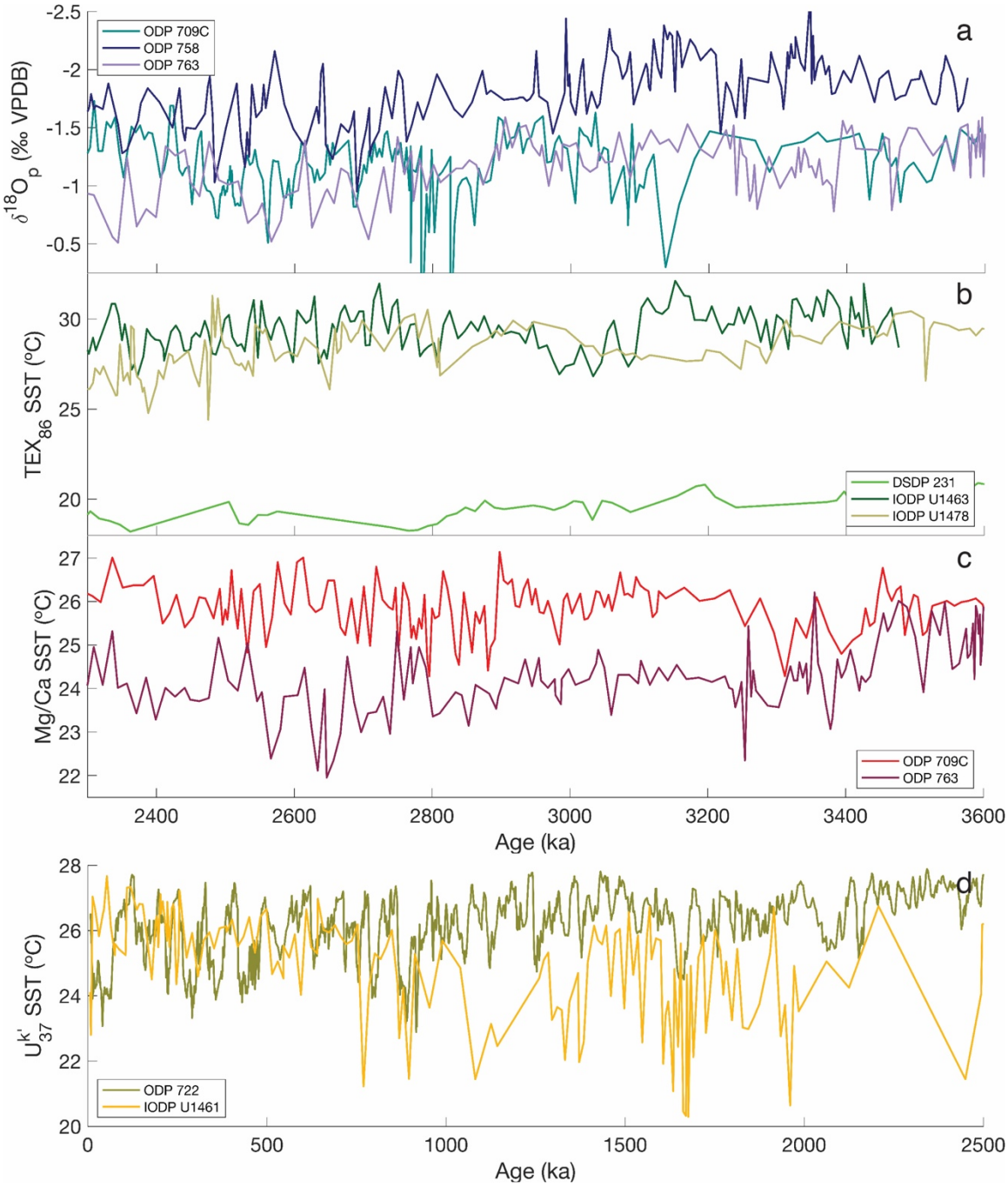

Figure S8. (a) Planktonic foraminiferal $\delta^{18}O$ (Chen et al., 1995; Farrell & Janecek, 1991; Karas et al., 2011; Shackleton & Hall, 1990), (b) TEX_{86} **(Liddy et al., 2016; Smith & Castañeda, 2020; Taylor et al., 2021)**, and (c) Mg/Ca (Karas et al., 2011) SST records used to construct IO ΔSST_{W-E} in the Plio-Pleistocene and (d) $U^{k'}_{37}$ SSTs (He et al., 2021; Herbert et al., 2015) used to construct Pleistocene ΔSST_{W-E}.

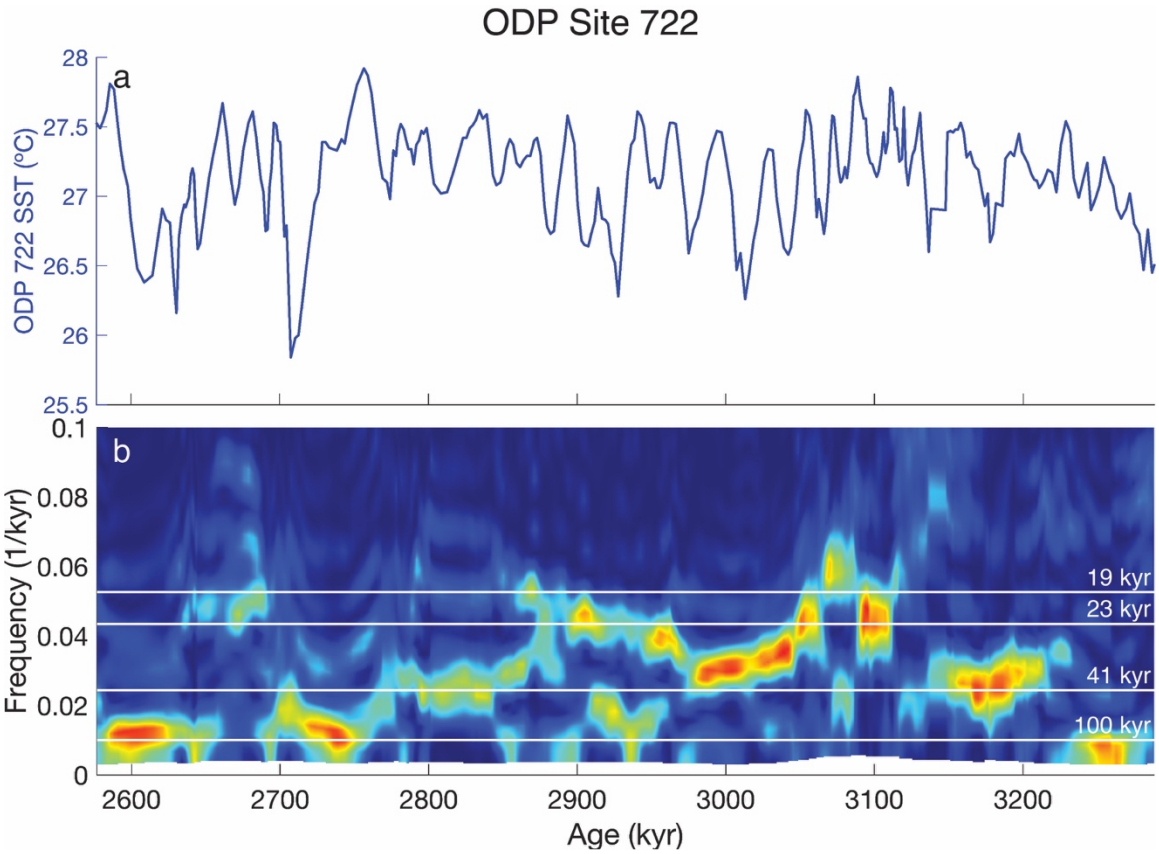

Figure S9. (a) ODP Site 722 $U^{k'}_{37}$ SSTs (Herbert et al., 2015) and a (b) 30-point evolutionary Lomb-Scargle periodogram of Site 722 SSTs.

References

Chen, J., Farrell, J. W., Murray, D. W., & Prell, W. L. (1995). Timescale and paleoceanographic implications of a 3.6 m.y. Oxygen isotope record from the northeast Indian Ocean (Ocean Drilling Program Site 758). *Paleoceanography*, *10*(1), 21–47. https://doi.org/10.1029/94PA02290

Farrell, J., & Janecek, T. (1991). Late Neogene Paleoceanography and Paleoclimatology of the Northeast Indian Ocean (Site 758). *Proceedings of the Ocean Drilling Program, Scientific Results*, *121*, 297–355. https://doi.org/10.2973/ODP.PROC.SR.121.124.1991

He, Y., Wang, H., & Liu, Z. (2021). Development of the Leeuwin Current on the northwest shelf of Australia through the Pliocene-Pleistocene period. *Earth and Planetary Science Letters*, *559*, 116767. https://doi.org/10.1016/j.epsl.2021.116767

Herbert, T. D., Ng, G., & Cleaveland Peterson, L. (2015). Evolution of Mediterranean sea surface temperatures 3.5–1.5 Ma: Regional and hemispheric influences. *Earth and Planetary Science Letters*, *409*, 307–318. https://doi.org/10.1016/j.epsl.2014.10.006

Karas, C., Nürnberg, D., Tiedemann, R., & Garbe-Schönberg, D. (2011). Pliocene Indonesian Throughflow and Leeuwin Current dynamics: Implications for Indian Ocean polar heat flux. *Paleoceanography*, *26*(2). https://doi.org/10.1029/2010PA001949

Liddy, H. M., Feakins, S. J., & Tierney, J. E. (2016). Cooling and drying in northeast Africa across the Pliocene. *Earth and Planetary Science Letters*, *449*, 430–438. https://doi.org/10.1016/j.epsl.2016.05.005

Lisiecki, L. E., & Raymo, M. E. (2005). A Pliocene-Pleistocene stack of 57 globally distributed benthic $\delta^{18}O$ records. *Paleoceanography*, *20*(1), n/a-n/a. https://doi.org/10.1029/2004PA001071

Martínez-Garcia, A., Rosell-Melé, A., McClymont, E. L., Gersonde, R., & Haug, G. H. (2010). Subpolar link to the emergence of the modern equatorial Pacific cold tongue. *Science*, *328*(5985), 1550–1553. https://doi.org/10.1126/science.1184480

Shackleton, N., & Hall, M. A. (1990). Pliocene oxygen isotope stratigraphy of Hole 709C. *Proceedings of the Ocean Drilling Program, Scientific Results*, *115*, 529–538. https://doi.org/doi:10.2973/odp.proc.sr.115.174.1990

Smith, R. A., & Castañeda, I. S. (2020). *NOAA/WDS Paleoclimatology—Eastern Indian Ocean Biomarker Data and Sea Surface Temperature Reconstructions from 3.5—1.5 Ma* [dataset]. NOAA National Centers for Environmental Information. https://doi.org/10.25921/E1P0-9T22

Taylor, A. K., Berke, M. A., Castañeda, I. S., Koutsodendris, A., Campos, H., Hall, I. R., Hemming, S. R., LeVay, L. J., Sierra, A. C., O'Connor, K., & Scientists, E. 361. (2021). Plio-Pleistocene Continental Hydroclimate and Indian Ocean Sea Surface Temperatures at the Southeast African Margin. *Paleoceanography and Paleoclimatology*, *36*(3), e2020PA004186. https://doi.org/10.1029/2020PA004186

Westover, K. S., Stone, J. R., Yost, C. L., Scott, J. J., Cohen, A. S., Rabideaux, N. M., Stockhecke, M., & Kingston, J. D. (2021). Diatom paleolimnology of late Pliocene Baringo Basin (Kenya) paleolakes. *Palaeogeography, Palaeoclimatology, Palaeoecology*, *570*, 109382. https://doi.org/10.1016/j.palaeo.2019.109382